CELL BIOLOGY – IMMUNOLOGY – PATHOLOGY

Catalase deficiency renders remnant kidneys more susceptible to oxidant tissue injury and renal fibrosis in mice

MIZUHO KOBAYASHI, HITOSHI SUGIYAMA, DA-HONG WANG, NAOMI TODA, YOHEI MAESHIMA, YASUSHI YAMASAKI, NORIYOSHI MASUOKA, MASAO YAMADA, SHOHEI KIRA, and HIROFUMI MAKINO

Department of Medicine and Clinical Science, Okayama University Graduate School of Medicine and Dentistry, Okayama, Japan; Department of Virology, Okayama University Graduate School of Medicine and Dentistry, Okayama, Japan; Department of Public Health, Okayama University Graduate School of Medicine and Dentistry, Okayama, Japan; and Department of Biochemistry, Okayama University Graduate School of Medicine and Dentistry, Okayama, Japan

Catalase deficiency renders remnant kidneys more susceptible to oxidant tissue injury and renal fibrosis in mice.

Background. Catalase is one of the important antioxidant enzymes regulating the levels of intracellular hydrogen peroxide and hydroxyl radical. The effect of catalase deficiency on progressive renal fibrosis has not been fully elucidated.

Methods. Homozygous acatalasemic mutant mice (C3H/AnLCs^{b}Cs^b) and control wild-type mice (C3H/AnLCs^{a}Cs^a) were subjected to 5/6 nephrectomy. The functional and morphological alterations of the remnant kidneys, including tubulointerstitial fibrosis, epithelial to mesenchymal transition (EMT), peroxidation, antioxidant enzyme activity, and gene expression of EMT-related molecules were compared between the two groups at 6, 12, and 18 weeks after 5/6 nephrectomy.

Results. The 5/6 nephrectomy resulted in albuminuria, decreased renal function, and tubulointerstitial fibrosis with accumulation of type I and type IV collagens in the remnant kidneys of both mouse groups. However, the degree of these changes was significantly higher in acatalasemic mice after 5/6 nephrectomy as compared with wild-type mice until week 18. EMT, a crucial phenotypic alteration of tubular epithelial cells, was observed in acatalasemic mice by electron microscopy and was associated with upregulation of EMT-related α-smooth muscle actin (α-SMA), transforming growth factor-β1 (TGF-β1), connective tissue growth factor (CTGF), and fibroblast specific protein-1 (FSP-1) gene expression. Significant increases in the tubulointerstitial deposition of lipid peroxidation products, including 4-hydroxy-2-nonenal and urinary excretion of 8-hydroxy-2′- deoxyguanosine were observed in the acatalasemic mice after 5/6 nephrectomy as compared with the wild-type mice. Glomerular sclerosis developed after tubulointerstitial injury in acatalasemic mice. The level of catalase activity remained low in the remnant kidneys of acatalasemic mice until week 18 without compensatory up-regulation of glutathione peroxidase or superoxide dismutase (SOD) activity. Finally, supplementation of a SOD mimetic tempol did not prevent peroxidation and tubulointerstitial fibrosis in the acatalasemic remnant kidneys.

Conclusion. These findings indicate that acatalasemia exacerbates renal oxidant tissue injury and sensitizes remnant kidneys to EMT and progressive renal fibrosis. This study suggests a central role for catalase in the defense against oxidant-mediated renal fibrosis.

Oxidant-mediated tissue injury plays an important role in the development and progression of major organ fibrosis, including the heart, liver [1], and pancreas [2]. The degree of oxidative stress and the severity of subsequent organ fibrosis have been postulated to depend on the imbalance between excess production of reactive oxygen species (ROS) and the antioxidant defense system within the tissue [3]. These antioxidants include the enzymes superoxide dismutase (SOD), catalase, and glutathione peroxidase, which detoxify ROS. Overexpression of glutathione peroxidase has been shown to inhibit oxidant tissue injury such as cardiac fibrosis [4]. The kidney has a high rate of oxidative metabolism as evidenced by the fact that the intact kidneys which represent less than 1% of the total body weight, nevertheless account for approximately 10% of the total oxygen consumption, putting the renal tubulointerstitium at continuous risk of oxidant tissue injury.

Catalase is a major enzyme that catalyzes the decomposition of hydrogen peroxide (H_2O_2) and plays a role in cellular antioxidant defense mechanisms [5]. The enzyme is localized in the matrix of peroxisomes in mammalian cells and is involved in two different types of enzymatic reactions: the catalatic mode ($2H_2O_2 \rightarrow O_2 + 2 H_2O$) and the peroxidatic mode ($H_2O_2 + AH_2 \rightarrow A + 2 H_2O$) [6]. Catalase thus limits the accumulation of H_2O_2, which is generated by various oxidases in tissue and serves as a substrate for the Fenton reaction to generate the highly injurious hydroxyl radical. Genetic defects of catalase were first documented by Takahara [7] and

Ogata [8] in Japanese patients who exhibited a deficiency of blood catalase enzyme activity (acatalasemia). Short-term clinical manifestations in acatalasemic patients appear predominantly in the mouth after exposure to H_2O_2 or infection with peroxide-generating bacteria such as streptococci and pneumococci, and the related activity of phagocytic cells at inflamed sites.

Subsequently, an acatalasemic mouse strain (Cs^b) was established by Feinstein, Suter, and Jaroslow [9] from the progeny of x-ray–irradiated mice. The tissues of acatalasemic mice express normal catalase mRNA levels compared with those of wild-type mice, suggesting the mutation does not act at the level of gene transcription or mRNA stability, but rather at the level of mRNA translation and/or protein turnover [10]. The mutation has been mapped to the mouse catalase structural gene on chromosome 2 (*Cat* or *Cas1*) and is expressed by modification of the enzyme active site but not of the antigenic site [9]. Recently, a new line of catalase null mice has been generated by a gene targeting technique [11]. Unexpectedly, homozygous *Cat* knockout mice are not more vulnerable to hypoxia-induced lung injury, nor do their lenses exhibit any increased susceptibility to oxidant-mediated injury. However, they are susceptible to brain injury following physical trauma causing a significant decrease in mitochondrial electron transfer [11], indicating a differential pattern of oxidant sensitivity in the types of tissue from *Cat* mutant mice. Since patients with acatalasemia have residual catalase activity in tissues, the mouse phenotype of complete *Cat* gene knockout may not reflect the human acatalasemic conditions.

Deterioration of renal function is largely determined by the degree of tubulointerstitial changes rather than by the extent of histologic changes in the glomeruli in many forms of renal disease [12]. Creatinine clearance or the glomerular filtration rate (GFR) correlates better with indices of tubulointerstitial damage than with those of glomerular injury [13]. Indeed, damage to the tubulointerstitium causes changes in the extracellular matrix (ECM) and leads to a remodeling of the tubulointerstitial structure [14]. The ECM of the tubulointerstitium in progressive renal disease increases, which eventually leads to irreversible fibrosis of the kidney. Renal fibrosis is characterized by the loss of renal tubules and interstitial capillaries as well as the accumulation of ECM proteins, such as collagen types I, II, IV, V, VII, fibronectin, and laminin [12]. Increased myofibroblasts and inflammatory cells have been identified as sources of the accumulated ECM in renal fibrosis [15]. However, the pathogenic mechanisms of renal interstitial ECM accumulation and fibrosis have not been fully elucidated yet.

Epithelial to mesenchymal transition (EMT) is a key phenotypic alteration of renal tubular epithelial cells (TECs) transdifferentiated into fibroblasts. Pioneering studies by Strutz et al [16] indicated that TECs could express fibroblast-specific markers in renal diseases, suggesting a central role of EMT in renal tubulointerstitial fibrosis [16]. Subsequently, a growing body of evidence has indicated that a large proportion of up to one third of interstitial fibroblasts originate from TECs via EMT in disease states [17]. Both the pro- and antifibrotic molecules are believed to play roles in the regulation of the fibrogenic process, including EMT. In particular, transforming growth factor-β1 (TGF-β1) [18] and connective tissue growth factor (CTGF) [19] are considered to promote fibrosis; in contrast, bone morphogenic protein 7 (BMP-7) [17, 20] and hepatocyte growth factor (HGF) [21] counteract profibrotic responses. However, other intracellular mediators may play important roles as well. Indeed, a recent report suggests that the increase in ROS by catalase deficiency may be involved in renal fibrosis after unilateral ureteral obstruction (UUO) [22]. In that report, however, the role of ROS in mediating tubular EMT and the expression of EMT-related genes was not investigated. The role of ROS in mediating tubular EMT and subsequent renal fibrosis is currently largely unknown.

In the present study, we hypothesized that a defect in the antioxidant system in the form of catalase deficiency would enhance oxidant tissue injury, renal tubular EMT, and interstitial fibrosis, eventually leading to the loss of renal function. This hypothesis was tested by inducing 5/6 nephrectomy, which is a well-established model of progressive renal fibrosis, into acatalasemic mice. Moreover, the effect of tempol, a membrane-permeable SOD mimetic, on oxidant-mediated renal fibrosis in acatalasemia was also investigated. The data presented here suggest that acatalasemia promotes renal fibrosis via the acceleration of tubular EMT in association with an elevation of EMT-related genes.

METHODS

Experimental animal protocol

Male wild-type mice (C3H/AnLCs^{a}Cs^a) and male homozygous acatalasemic mutant mice (C3H/AnLCs^{b}Cs^b) were used at the age of 7 to 10 weeks old. Animals were housed in a group of five and fed standard chow and water ad libitum. Renal ablation was induced by the pole resection protocol with the mice under pentobarbital anesthesia as described previously [23, 24]. Mice were divided into subgroups ($N = 10$/group). Body weight was measured every 6 weeks until 18 weeks. Arterial blood pressure was measured every 6 weeks using a programmable sphygmomanometer (BP-98A) (Softron, Tokyo, Japan) by the tail-cuff method as described previously [24, 25]. Mean blood pressure was calculated as (systolic pressure + 2 × diastolic pressure)/3. Twenty-four hour urine samples were collected in metabolic cages. Mice that were operated on were sacrificed under pentobarbital anesthesia 0 ($N = 10$), 6 ($N = 10$), 12

($N = 10$), and 18 ($N = 10$) weeks after 5/6 nephrectomy. Sham operation, in which mice had their kidneys manipulated but not nephrectomized, was also performed on both wild-type and acatalasemic mice ($N = 10$ in each time point) [23, 24]. Immediately before death, blood samples were drawn from the retro-orbital sinus. Three acatalasemic mice but none of wild-type mice died after 5/6 nephrectomy during the experimental period. In tempol-treated groups, mice received continuous infusion of tempol (4-hydroxy-2,2,6,6-tetramethylpiperidine-N-oxyl, 100 mg/kg body weight/day) (Sigma Chemical Co., St. Louis, MO, USA) via subcutaneous osmotic minipumps (Alzet model 2004) (Alza Corp., Palo Alto, CA, USA) over a 8-week period from 5 to 12 weeks after 5/6 nephrectomy. The minipumps were replaced with new ones at 4 weeks after the first implantation. The experimental protocol was approved by the Ethics Review Committees for Animal Experimentation of Okayama University Graduate School.

Blood and urine examination

Serum creatinine, blood urea nitrogen (BUN), thiobarbituric acid reactive substance (TBARS), urinary creatinine levels, and urinary albumin excretion were measured as described previously [22]. Creatinine clearance was calculated in individual mice as μL/min/g body weight. As a marker for oxidative DNA damage, we measured the urinary excretion of 8-hydroxy-2′-deoxyguanosine (8-OHdG) in a 24-hour urine collection by enzyme-linked immunosorbent assay (ELISA) using the 8-OHdG ELISA Kit (Japan Institute for the Control of Aging, Shizuoka, Japan) as recommended by the manufacturer [26]. Absorbance was measured at 540 nm using a microplate reader (model 550) (Bio-Rad, Hercules, CA, USA).

Reagents and antibodies

Chemicals and reagents of analytic grade were purchased from Sigma Chemical Co. or Wako Pure Chemical Ind. (Osaka, Japan) unless stated. *meso*-Tetrakis (1-methyl-4-pyridyl)-porphyrin was purchased from Dojindo Labs (Kumamoto, Japan). The following primary antibodies were used for immunohistochemistry: mouse monoclonal antibodies to 4-hydroxy-2-nonenal (4-HNE) [26] or 4-hydroxy-2-hexenal (4-HHE) were obtained from Nof Life Science (Tokyo, Japan), biotinylated *Arachis hypogaea* peanut agglutinin from Vector Laboratories, Inc. (Burlingame, CA, USA), rabbit polyclonal antibodies against type I collagen and type IV collagens from Chemicon International Inc. (Temecula, CA, USA).

Light and electron microscopic studies

Remnant or control kidneys were removed, fixed in 10% buffered formalin, and embedded in paraffin. Paraffin sections (3 μm thick) were stained with periodic acid-Schiff (PAS), Masson trichrome, and Azan-Mallory staining [22–24, 27]. Two independent observers with no prior knowledge of the experimental design evaluated each tissue section by an Olympus light microscope (Olympus, Tokyo, Japan) with high-resolution digital camera systems (Penguin 600CL) (Pixera Co., Los Gatos, CA, USA). The diameter of glomeruli, spanning from the vascular pole to the opposite Bowman's capsule, was measured using a Microanalyzer program (version 1.1) (Japan Poladigital Co., Tokyo, Japan). Glomerular sclerosis was graded as follows: 0, none; +1, sclerotic changes in <25% of the glomerulus; +2, from 25% to 50%; and +3, >50% [23, 24]. The mean score per glomerulus in each kidney was determined as the sclerosis index. More than 30 glomerular cross sections were examined by two investigators and averaged. The observers scored with a semiquantitative scale designed to evaluate the degree of tubulointerstitial injuries, including tubular atrophy and interstitial fibrosis in Masson trichrome stain [22]. The tubulointerstitial fibrosis score ranging from 0 to 4 was determined as follows: 0, normal kidney; 1, mild change; 2, moderate change; 3, severe change; and 4, whole tissue was injured. The scores were determined in each section selected at random and more than 20 fields were examined under ×100 magnification. Electron microscopy was performed in the mouse kidney specimens as described previously [22, 28]. In brief, tissue blocks of kidney sections were immersed in 2.5% glutaraldehyde for 2 hours at 4°C and postfixed with 1% osmium tetroxide. The blocks were then processed for routine dehydration, epon embedding, and thin sectioning, and examined with an electron microscope (Hitachi, Tokyo, Japan). The quantitative analysis was performed to count the number of actin bundle–positive TECs and total TECs in each sample by electron microscopy. The mean percentage of actin bundle–positive TECs per total TECs was determined.

Immunohistochemical studies

Deposition of lipid peroxidation products in renal tubulointerstitium were examined by immunoperoxidase staining as described previously [22]. Briefly, formalin-fixed, paraffin-embedded sections were deparaffinized, and endogenous peroxidase was inactivated with 0.3% H_2O_2. Unfixed cryostat sections (4 μm thick) were prepared for the staining of α-smooth muscle actin (α-SMA). Sections were then washed in phosphate-buffered saline (PBS) three times, 5 minutes each, preincubated in a blocking solution (10% goat serum in PBS) for 30 minutes, washed in PBS three times, and then incubated for 1 hour at room temperature or overnight at 4°C with primary antibodies. Sections using control kidneys were treated similarly but without addition of the primary antibody. Each section was washed three times in PBS and

Table 1. Primer sequences, product sizes, and conditions for real-time PCR analysis

	Sense primer	Antisense primer	Product size *bp*	GenBank accession number	Annealing temperature	Cycle number
TGF-β1	5′-AACAACGCCATCTATGAG	5′-TATTCCGTCTCCTTGGTT	294	NM_011577	61	40
CTGF	5′-AAGACCTGTGGGATGGGC	5′-GTGCAGCCAGAAAGCTCA	191	BC006783	62	40
α-SMA	5′-GACAGGATGCAGAAGGAGAT	5′-TTAGAAGCATTTGCGGTG	198	BC064800	62	40
FSP-1	5′-CAGGCAAAGAGGGTGACAAG	5′-TGCAGGACAGGAAGACACAG	186	NM_011311	62	40
GAPDH	5′-TGAACGGGAAGCTCACTGG	5′-TCCACCACCCTGTTGCTGTA	307	NM_001001303	60	40

Abbreviations are: TGF-β1, transforming growth factor beta-1; CTGF, connective tissue growth factor; α-SMA, α-smooth muscle actin; FSP-1, fibroblast specific protein-1; GAPDH, glyceraldehyde-3-phosphate dehydrogenase.

then incubated with the second antibody for 30 minutes. Biotinylated rabbit antimouse IgG (Nichirei Corp., Tokyo, Japan) (dilution 1:1000) was used as the second antibody. After the sections were washed with PBS three times, they were placed in peroxidase-labeled streptavidin (Nichirei Corp.). They were placed in diaminobenzidine/H_2O_2 solution, counterstained with hematoxylin, dehydrated, and enclosed in synthetic resin. Peroxidation products were determined on the basis of the intensity and distribution of deposition in the tubulointerstitium: 0, none or trace staining; 1, mild; 2, moderate; and 3, severe staining. The score was determined in 20 randomly selected nonoverlapping ×200 fields in each section of the individual mouse renal cortex. The average number of score from ten separate animals was calculated.

Indirect immunofluorescence was performed as described previously [22, 24, 27]. Briefly, surgically removed kidney specimens were immediately snap-frozen and unfixed cryostat sections (4 μm thick) were prepared. The sections were washed in PBS three times, 5 minutes each, and then incubated with rabbit polyclonal antibodies against type I, type III, or type IV collagen (dilution 1:50) as the primary antibody in PBS for 1 hour at room temperature. Each section was washed three times in PBS and incubated with fluorescein isothiocyanate (FITC)-conjugated goat antirabbit IgG (Zymed Laboratories, Inc., San Francisco, CA, USA) (dilution 1:100) as the second antibody in PBS for 30 minutes. After the section was washed with PBS three times, it was mounted with fluoromount-G. Deposition of type I, III, or IV collagens in the tubulointerstitium of renal cortex was assessed semiquantitatively by fluorescence microscopy as described previously [22, 27]. The collagen deposition score was determined on the basis of the intensity and distribution of each collagen in the tubulointerstitium: 0, none; 1, trace; 2, mild; 3, moderate; and 4, severe staining. The score was determined in each section selected at random and more than 20 fields were examined under ×100 magnification.

Extraction of total RNA and quantitative real-time polymerase chain reaction (PCR) analysis

Total RNA was extracted from the whole kidney by using an RNeasy Midi Kit using the instructions provided by the manufacturer (Qiagen, Valencia, CA, USA) and quantified by measuring absorbance at 260 nm and stored at −80°C until assay [24, 27]. Two micrograms of total RNA from each sample was used for reverse transcription (RT) using a GeneAmp RNA PCR kit (Applied Biosystems, Foster City, CA, USA) with random hexamer (2.5 μmol/L), murine leukemia virus reverse transcriptase (50 U), and deoxyribonucleoside triphosphate (1 mmol/L) at 42°C for 15 minutes, 99°C for 5 minutes, and then 5°C for 5 minutes [29]. For the quantification of mRNA levels of EMT-related genes, real-time PCR was performed using LightCycler-FastStart DNA master SYBR Green I system (Roche Diagnostics, Mannheim, Germany). Oligonucleotides used for real-time PCR to quantify the amounts of TGF-β1, CTGF [30], α-SMA [31], fibroblast specific protein-1 (FSP-1) (S100 calcium binding protein A4) [32], and glyceraldehyde-3-phosphate dehydrogenase (GAPDH) were customordered from Nihon Gene Research Lab Inc. (Sendai, Miyagi, Japan). Sequences of the mouse primer pairs and the original clones are listed in Table 1. After RT, cDNA was diluted 1:10 with autoclaved deionized water and 5 μL of the diluted cDNA was added to the Lightcycler-Mastermix (0.5 μmol/L of specific primer, 3 mmol/L $MgCl_2$ and 2 μL Master SYBR Green) (Roche Diagnostics). This reaction mixture was filled up with water to a final volume of 20 μL. PCR reactions were carried out in a real-time PCR cycler (Lightcycler) (Roche Diagnostics) and analyzed using Roche Molecular Biochemicals Lightcycler Software version 3.5 (Roche Diagnostics). The program was optimized and performed finally as denaturation at 95°C for 10 minutes followed by 40 cycles of amplification (Table 1). The temperature ramp rate was 20°C per second. At the end of each extension step, the fluorescence of each sample was measured to allow the quantification of the PCR product. After completion of the PCR, the melting curve of the product was measured by temperature gradient from 60 to 95°C at 0.2°C per second with continuous fluorescence monitoring to produce a melting profile of the primers. The amount of PCR products was normalized with GAPDH to determine the relative expression ratios for each mRNA in relation to GAPDH mRNA. RT-PCR experiments were repeated twice under identical conditions to verify the results.

Table 2. Metabolic data

Group	0 week	6 weeks	12 weeks	18 weeks
Body weight *g*				
Wild-type 5/6 nephrectomy	27.4 ± 0.4	31.2 ± 0.7^c	32.7 ± 0.6^b	37.0 ± 1.1^a
Acatalasemic 5/6 nephrectomy	26.2 ± 0.5	29.9 ± 0.9^d	31.4 ± 1.5^c	30.3 ± 1.7^d
Relative kidney weight *mg/g body weight*				
Wild-type 5/6 nephrectomy	9.0 ± 0.4	6.3 ± 0.4^c	6.7 ± 0.5^c	6.6 ± 0.3^c
Acatalasemic 5/6 nephrectomy	9.4 ± 0.3	6.6 ± 0.2^b	$6.1 \pm 0.5^{b,d}$	6.4 ± 0.4^b
Mean blood pressure *mm Hg*				
Wild-type 5/6 nephrectomy	77.4 ± 2.4	81.7 ± 2.3	81.0 ± 2.8	78.8 ± 3.0
Acatalasemic 5/6 nephrectomy	76.3 ± 3.6	81.3 ± 2.6	87.1 ± 3.1	82.8 ± 4.1

Values are means $\pm$ SE (g) of 8 to 10 animals in each group.
[a] $P < 0.001$; [b] $P < 0.01$; [c] $P < 0.05$ vs. 0 week in the same group; [d] $P < 0.05$ vs. wild-type 5/6 nephrectomy group at the same time point.

Renal catalase, glutathione peroxidase, and SOD activity

When kidneys were harvested, each kidney was decapsulated, washed with saline, bisected coronally, blotted dry on gauze, and weighed as described previously [22, 24, 27]. The whole kidney weight was expressed as a percentage of body weight determined at the time the mice were sacrificed. Dried kidney weight was not determined. After harvesting obstructed or contralateral kidney from either wild or acatalasemic mice, samples were stored in –80°C freezer until assay. Catalase activity was determined by measuring the removal rate of 70 µmol/L H_2O_2 based on the method of Sunami et al [22] and Masuoka et al [33, 34]. Samples, including renal cortex, were homogenized with a Teflon homogenizer in homogenization buffer [0.1 mol/L potassium phosphate buffer (PPB) (pH 7.2) containing 1 mmol/L ethylenediaminetetraacetic acid (EDTA), and 1% Triton X-100]. The samples were centrifuged for 30 minutes (11,000 $\times$ *g*) at 4°C. The supernatant was removed and diluted with 0.1 mol/L PPB to make 0.2% homogenate. Then, 0.2 mL of 3.5 mmol/L H_2O_2 was added and after 0, 30, and 60 seconds, 2 mL of the reaction mixture (containing less than 140 nmol of H_2O_2) was taken out and put into the test tubes containing 2 mL of the reagent solution [consisted of 10 volumes of 0.2 mmol/L *meso*-tetrakis(4-methylpyridyl)-porphinatoiron (III) pentachloride solution, 10 volumes of 41.2 mm *N,N*-dimethylaniline in 0.2 mol/L hydrochloric acid, 10 volumes of 8.56 mmol/L 3-methyl-2-benzothiazolinone hydrazone solution in 0.2 mol/L hydrochloric acid and 1 volume of 20 mmol/L EDTA solution]. The mixture was incubated at 25°C for 1 h, and then the absorbance at 590 nm was measured.

Glutathione peroxidase activity was determined by the method as described previously [35] with some modification. The assay is an indirect measure of the activity of cellular glutathione peroxidase. Oxidized glutathione is recycled to its reduced form by glutathione reductase. The oxidation of nicotinamide adenine dinucleotide phosphate (NADPH) resulting NADP+ is accompanied by a decrease in absorbance at 340 nm so that glutathione peroxidase activity can be monitored. To assay glutathione peroxidase, tissue homogenate was added to a solution containing glutathione, glutathione reductase and NADPH. The enzyme reaction was started by adding tert-butyl hydroperoxide as a substrate and the 340 nm absorbance was recorded every 5 seconds for 1 minute. The rate of decrease in the 340 nm absorbance was directly proportionate to glutathione peroxidase activity in the sample. The activity of SOD was measured as described by Sutherland and Learmonth [36] using an SOD assay kit (Trevigen, Gaithersburg, MD, USA) [37]. This method is based on the inhibition of the reduction of nitro blue tetrazolium by SOD. Superoxide ions convert nitro blue tetrazolium into blue formazan. Blue formazan absorbs light at 550 nm. SOD reduces the superoxide ion concentration and thereby lowers blue formazan formation. The extent of reduction in the appearance of blue formazan reflects the amount of SOD activity in a sample.

Statistical analyses

Data, shown as mean $\pm$ SEM, were analyzed by the Mann-Whitney U test or one-way analysis of variance (ANOVA) using the StatView program (Hulinks, Tokyo, Japan). P values < 0.05 were accepted as statistically significant.

RESULTS

Changes in body weight, kidney weight, and arterial blood pressure in the mouse remnant kidney model

The remnant kidney model has been extensively studied in many different rat strains. In contrast, mice have generally been resistant to this model, particularly in animals of the C57BL/6 background [38]. Therefore, we first tried to characterize this model in our mouse strains. Male acatalasemic mice were found on observation to grow normally and were apparently healthy up to 1 year of age. Female acatalasemic mice were as fertile as wild-type mice. The morphology of major organs, including the heart, lung, liver, and kidney, appeared normal upon histologic examination at the level of light microscopy. Body weight and relative kidney weight were similar between both groups at the start of the experiment (Table 2).
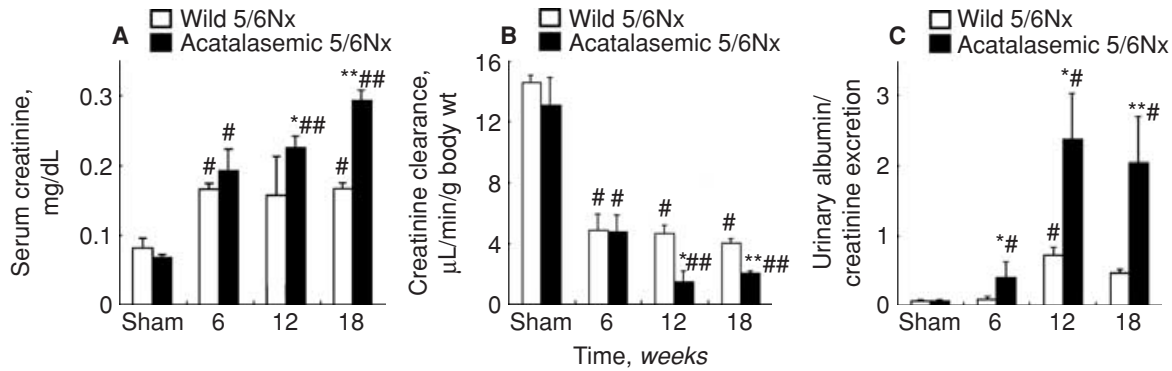
Fig. 1. Changes in renal function and urinary albumin excretion in wild-type (□) and acatalasemic mice (■). (*A*) Serum creatinine significantly increased in both groups at 6 weeks after 5/6 nephrectomy (5/6Nx). The elevation of serum creatinine in acatalasemic mice is remarkable at 12 and 18 weeks after 5/6 nephrectomy as compared to that in wild-type mice. (*B*) Creatinine clearance markedly decreased in both groups at 6 weeks after 5/6 nephrectomy. In acatalasemic mice, the decrease in creatinine clearance was significantly more than that in wild-type mice at 12 and 18 weeks after 5/6 nephrectomy. (*C*) Daily urinary albumin to creatinine excretion ratio. The 5/6 nephrectomy significantly increased urinary albumin exrection in acatalasemic mice at 6 weeks but not in wild-type mice. Urinary albumin excretion remarkably increased in acatalasemic group after 12 weeks. Each column consists of means ± SE ($N = 7$ to 10 animals/group). *$P < 0.05$; **$P < 0.01$ vs. wild-type 5/6 nephrectomy mice at the same time point; #$P < 0.05$; ##$P < 0.01$ vs. sham at 0 week in the same group.

A significant increase in body weight was observed at 6, 12, and 18 weeks in the wild-type 5/6 nephrectomy mice, while an increase in body weight of the acatalasemic mice after 5/6 nephrectomy was not observed at time points later than 12 weeks. The decrease in the kidney weight to body weight ratio was observed in both groups and it was significant in acatalasemic 5/6 nephrectomy at 12 weeks as compared to that in wild-type 5/6 nephrectomy. Arterial blood pressure in acatalasemic 5/6 nephrectomy slightly increased at 12 weeks, without a significant difference from that in acatalasemic control or wild-type 5/6 nephrectomy at the same time point (Table 2).

Increase in albuminuria and decrease in renal function are significantly accelerated in acatalasemic mice after 5/6 nephrectomy

To evaluate the effect of acatalasemia on 5/6 nephrectomy–induced alteration of biologic functions, we measured parameters of renal function (serum creatinine and creatinine clearance) and daily urinary albumin excretion (Fig. 1). The basal levels of serum creatinine, creatinine clearance, urinary albumin excretion were not significantly different between the wild-type and acatalasemic mice. In both groups, significant increases in serum creatinine and decreases in creatinine clearance were observed after 5/6 nephrectomy, but they were more severe in acatalasemic 5/6 nephrectomy mice compared with wild-type 5/6 nephrectomy mice at the time points later than 6 weeks (Fig. 1A and B). A significant elevation of urinary albumin excretion was observed in acatalasemic mice as compared to wild-type mice after 5/6 nephrectomy (Fig. 1C).

Acatalasemia accelerates periglomerular fibrosis and increases expression of type I and type IV collagens in tubulointerstitium of remnant kidneys

In wild-type and acatalasemic sham-operated mice, no histologic abnormalities of the kidneys were observed at the light microscopic level (Fig. 2A and B). In acatalasemic mice after 5/6 nephrectomy, tubulointerstitial fibrosis developed, especially in the periglomerular area in the deep cortex rather than the superficial cortex, and it significantly increased as compared with that in wild-type mice throughout the experiment (Fig. 2C, D, and M). To examine which ECM components increase in acatalasemic remnant kidneys, tubulointerstitial expression of type I and type IV collagens was investigated by immunohistochemistry. In the acatalasemic group, tubulointerstitial type I and type IV collagens were elevated at 6 weeks after 5/6 nephrectomy and were significantly higher than those in the wild-type group at time points later than 6 weeks throughout the experiment (Fig. 2N and O). A marked increase in de novo expression of type I collagen was observed in the interstitial expansion of acatalasemic 5/6 nephrectomy as compared with wild-type 5/6 nephrectomy (Fig. 2E and F). Type IV collagen was normally expressed in the glomerular and tubular basement membrane in both control kidneys (Fig. 2G and H). The increase in type IV collagen was more prominent in the acatalasemic remnant kidneys as compared to the wild-type remnant kidneys at 18 weeks after 5/6 nephrectomy (Fig. 2I and J). After 5/6 nephrectomy, kidney sections from wild-type mice exhibited glomerular hypertrophy and glomerular sclerosis (Table 3). In acatalasemic mice after 5/6 nephrectomy, the degree of glomerular sclerosis was more severe after 12 and 18 weeks as compared to that in wild-type mice (Fig. 2K and L) (Table 3).
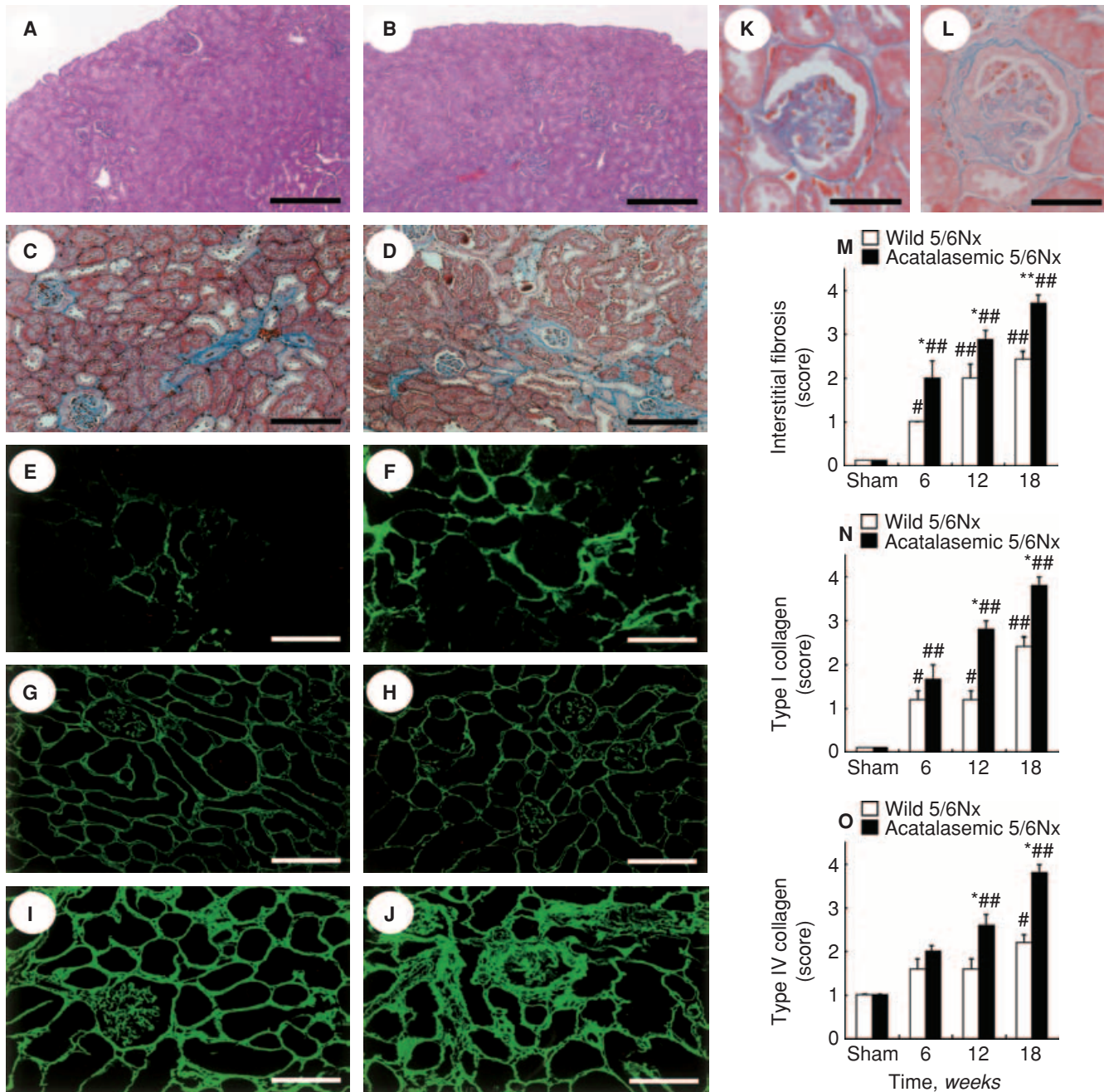
Fig. 2. Renal histology and deposition of tubulointerstitial collagens in wild-type and acatalasemic mice. Light micrographs of wild-type (*A*) and acatalasemic (*B*) sham-operated kidneys at 18 weeks, and wild-type (*C*) and acatalasemic (*D*) remnant kidneys at 18 weeks after 5/6 nephrectomy (5/6Nx). Note periglomerular tubulointerstitial fibrosis is significant in acatalasemic remnant kidneys compared with wild-type. Sham-operated kidneys are microscopically normal. Immunofluorescent micrographs of wild-type (*E*) and acatalasemic (*F*) remnant kidneys at 18 weeks stained with type I collagen, wild-type (*G*), and acatalasemic (*H*) sham-operated kidneys, and wild-type (*I*) and acatalasemic (*J*) remnant kidneys at 18 weeks stained with type IV collagen. Note increased de novo expression of type I collagen in interstitium of acatalasemic remnant kidneys. Tubulointerstitial type IV collagen is also accumulated in remnant kidneys of acatalasemic mice. Light micrographs of a glomerulus of wild-type (*K*) or acatalasemic (*L*) remnant kidneys at 18 weeks after 5/6 nephrectomy. Note significant glomerulosclerosis with periglomerular fibrosis develops in remnant kidneys of acatalasemic mice. Interstitial fibrosis score (*M*), type I collagen (*N*), and type IV collagen (*O*) deposition score of wild-type (□) or acatalasemic (■) mice (panels A and B, Masson-trichrome stain; panels C, D, J, and K, Azan stain). Scale bars are 400 (panels A and B), 200 (panels C and D), 100 (panels E to J), and 60 μm (panels K and L). In panels M to O, each column consists of means ± SE ($N = 7$ to 10 animals/group). *$P < 0.05$; **$P < 0.01$ vs. wild-type 5/6 nephrectomy mice at the same time point; #$P < 0.05$; ##$P < 0.01$ vs. sham at 0 week in the same group.

Table 3. Glomerular injury in remnant kidney model

Group	0 week	6 weeks	12 weeks	18 weeks
Diameter of glomerulus μ*m*				
Wild-type 5/6 nephrectomy	95.4 ± 2.6	100.0 ± 3.5	114.5 ± 1.3[c]	124.2 ± 2.1[b]
Acatalasemic 5/6 nephrectomy	91.9 ± 3.0	106.1 ± 6.7	119.7 ± 3.6[c]	130.0 ± 3.0[a]
Sclerosis index (score)				
Wild-type 5/6 nephrectomy	0.00 ± 0.00	0.17 ± 0.08	1.21 ± 0.26[b]	2.42 ± 0.17[a]
Acatalasemic 5/6 nephrectomy	0.00 ± 0.00	0.28 ± 0.04	1.62 ± 0.17[a]	2.80 ± 0.07[a,d]

Values are means ± SE of 8 to 10 animals in each group.
[a] $P < 0.001$; [b] $P < 0.01$; [c] $P < 0.05$ vs. 0 week in the same group; [d] $P < 0.05$ vs. wild-type 5/6 nephrectomy group at the same time point.
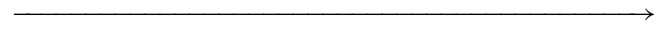
Acatalasemia sensitizes remnant kidneys to EMT via up-regulation of fibrosis-related genes

A morphologic study has suggested that TECs are able to acquire a myofibroblast phenotype and play an important role in the pathogenesis of renal fibrosis associated with 5/6 nephrectomy in rats [15]. Since we found an increase in the deposition of tubulointerstitial collagens in the acatalasemic remnant kidneys (Fig. 2), we further investigated whether acatalasemia activates tubular EMT in mice and studied the expression of fibrosis-related genes by electron microscopy and real-time PCR. In acatalasemic mice after 5/6 nephrectomy, TECs containing abundant actin microfilaments in their cytoplasm were observed adjacent to the interstitial fibrosis area (Fig. 3A and B). It was difficult to identify the segment of renal tubules containing actin microfilaments by electron microscopy, because such tubules lose their normal structural characteristics, including their cellular polarity, microvilli, and tight junctions. The percentage of TEC containing the actin bundles significantly increased in acatalasemic 5/6 nephrectomy mice (8.6 ± 0.8%) as compared with wild-type 5/6 nephrectomy mice at 18 weeks (2.8 ± 0.5%) ($P < 0.05$ vs. acatalasemic 5/6 nephrectomy mice). No cytoplasmic actin filaments were observed in the TECs of the control acatalasemic or wild-type kidney (data not shown). Immunohistochemical staining revealed that the expression of α-SMA protein in acatalasemic remnant kidneys was observed mainly in the interstitium (Fig. 3C) but also to some extent in TECs (Fig. 3D). Tubular EMT is regulated by the coordinated expression of a number of related genes. The kinetics of this gene expression revealed an early increase in α-SMA, a crucial marker for the transformation of cells to myofibroblasts, in acatalasemic mouse kidneys at 6 weeks after 5/6 nephrectomy (Fig. 3E). The gene expression of FSP-1, originally identified as specific for the fibroblast lineage, increased thereafter (Fig. 3F), suggesting differential regulation of the α-SMA and FSP-1 genes in renal fibrogenesis in acatalasemia. The gene expression of TGF-β1 and CTGF, key growth factors promoting tubular EMT in vitro and in vivo, significantly increased in the acatalasemic mice kidneys as compared with wild-type kidneys after 5/6 nephrectomy (Fig. 3G and H). The levels of gene expression of these fibrosis-promoting molecules were not significantly different between two sham-operated controls.

Renal and urinary peroxidation products increase in acatalasemia after 5/6 nephrectomy

We hypothesized that oxidative stress may be a factor in stimulating renal interstitial fibrosis in acatalasemic mice after 5/6 nephrectomy. Increased oxidative stress is known to damage to cellular macromolecules including nuclear DNA and membrane lipids. The major content of the cell membrane is lipid, and thus lipid peroxidation in tissues could cause renal injury. We next examined whether acatalasemia influenced lipid peroxidation products in the tubulointerstitial compartment of remnant kidneys. There was a mild increase in 4-HNE antibody labeling of various patches in the expansion of the interstitium in wild-type remnant kidneys as compared to sham-operated kidneys (Fig. 4A, C, and E). More intense

————————————————————→

Fig. 3. Ultrastructural evidence for the tubular epithelial to mesenchymal transition (EMT), expression of α-smooth muscle actin (α-SMA) protein in tubulointerstitium of acatalasemic remnant kidneys and expression of fibrosis-related genes after 5/6 nephrectomy (5/6Nx). Electron micrographs of tubular epithelial cells (TECs) demonstrating the early stage of EMT in acatalasemic mice at 18 weeks after 5/6 nephrectomy. (*A*) A TEC contains characteristic bundles of actin microfilaments (arrowheads) on the basal side of the tubular epithelial peripheral cytoplasm, lying parallel to partially disrupted (∗) tubular basement membranes. (*B*) Higher magnification of a bundle of actin microfilaments (arrowheads) within the cytoplasm of a tubular epithelia cell. Immunohistochemical staining of α-SMA in tubulointerstitium of acatalasemic mice at 18 weeks after 5/6 nephrectomy. (*C*) Significant staining is observed in the interstitium of acatalasemic remnant kidneys. (*D*) Higher magnification showing α-SMA–positive staining (arrowheads) on the basal side of the tubular epithelial cytoplasm in some areas. The renal mRNA expressions of α-SMA (*E*), fibroblast specific protein-1 (FSP-1) (*F*), transforming growth factor-β1 (TGF-β1) (*G*), and connective tissue growth factor (CTGF) (*H*) in wild-type (□) or acatalasemic (■) mice. Note acatalasemia significantly induced mRNA expression of α-SMA in remnant kidneys after 5/6 nephrectomy as compared to its mild induction in wild-type (*E*). Expression of EMT-related FSP-1 mRNA and profibrotic TGF-β1 and CTGF mRNA are moderately induced in acatalasemic 5/6 nephrectomy. The relative expression ratios for each mRNA in relation to glyceraldehyde-3-phosphate dehydrogenase (GAPDH_ mRNA) were determined. Each column consists of means ± SE ($N = 7$ to 10 animals/group). ∗$P < 0.05$ vs. wild-type 5/6 nephrectomy mice at the same time point; #$P < 0.05$; ##$P < 0.01$ vs. sham at 0 week in the same group. TL is tubular lumen. Scale bars are 2 (panel A), 1 μm (panel B), 100 μm (panel C), and 20 μm (panel D).
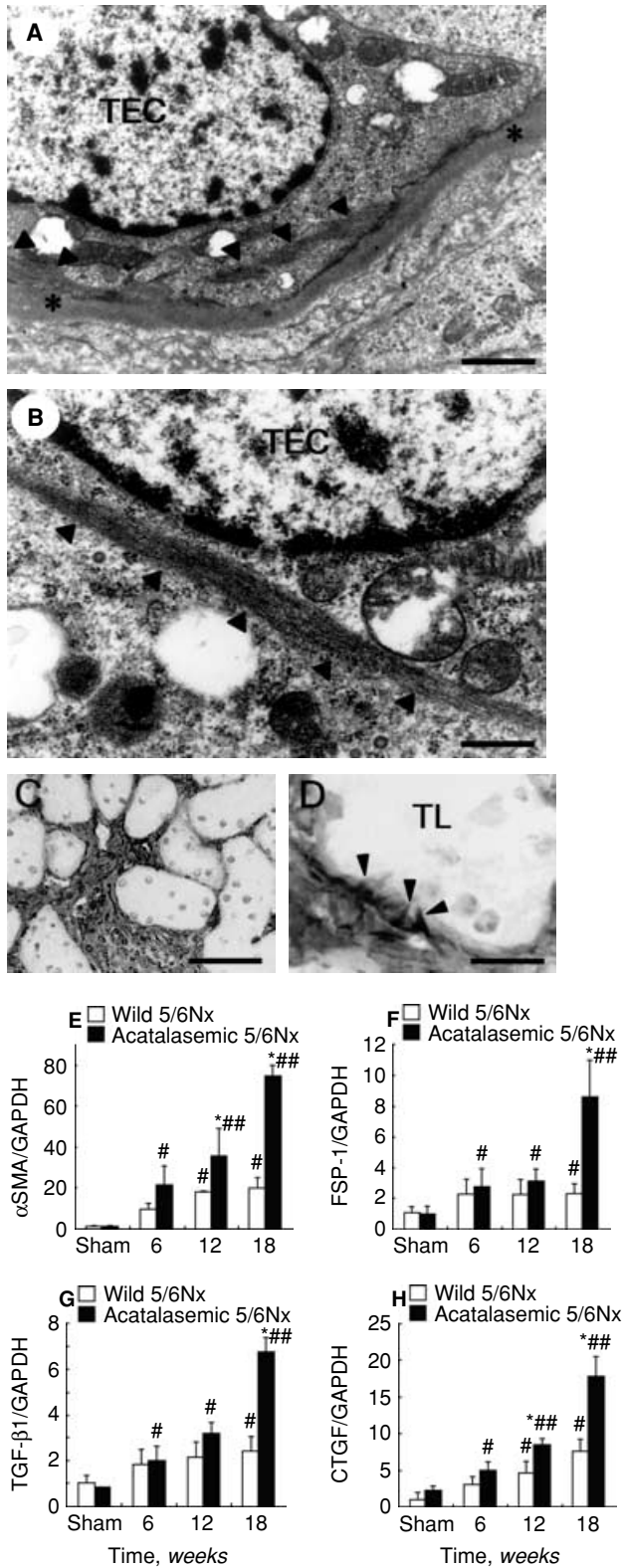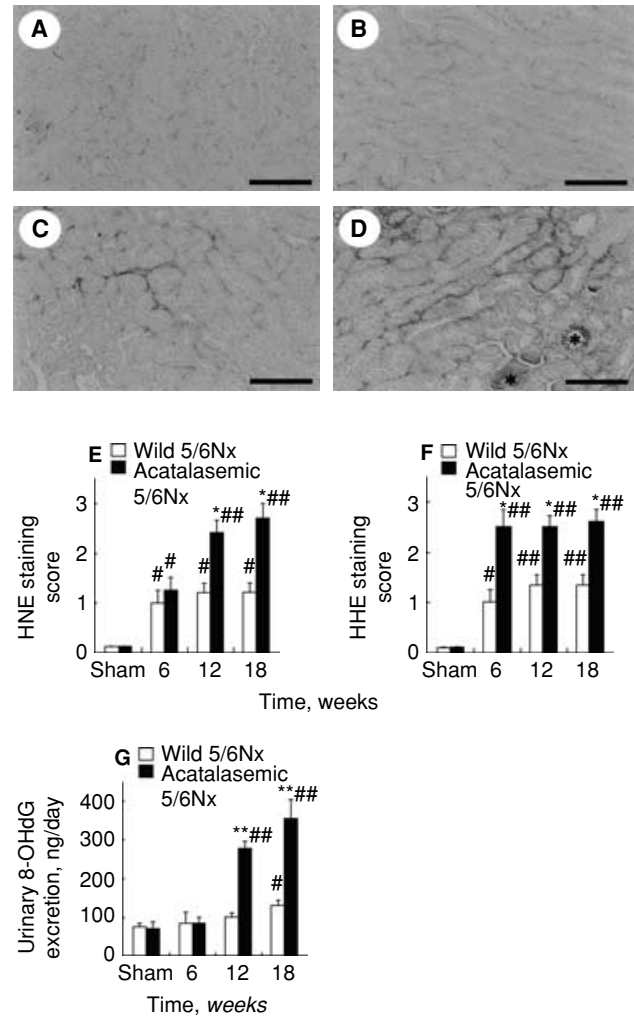
Fig. 4. Renal and urinary peroxidation products in wild-type and acatalasemic mice. Immunohistochemistry of lipid peroxidation products in renal tubulointerstitium in remnant kidneys of wild-type and acatalasemic mice. Light micrographs of staining of 4-hydroxy-2- nonenal (4-HNE)-modified proteins in wild-type (*A*) and acatalasemic (*B*) sham-operated kidneys, and wild-type (*C*) and acatalasemic (*D*) remnant kidneys at 18 weeks. Deposits of lipid peroxidation products are evident in interstitium and vessels (∗) of acatalasemic remnant kidneys (*D*). Accumulation of 4-HNE-modified (*E*) and 4-hydroxy-2-hexenal (4-HHE)-modified proteins (*F*) in kidneys is semiquantified in wild-type (□) and acatalasemic mice (■). Urinary 8-hydroxy-2′-deoxyguanosine (8-OHdG) excretion is markedly increased in acatalasemic 5/6 nephrectomy (5/6Nx) mice at time points later than 12 weeks as compared to wild-type 5/6 nephrectomy mice. Scale bars are 100 μm (panels A to D). In panels E to G, each column consists of means ± SE ($N = 7$ to 10 animals/group). $*P < 0.05$; $**P < 0.01$ vs. wild 5/6 nephrectomy at the same time point; $^#P < 0.05$; $^{##}P < 0.01$ vs. sham at 0 week in the same group.

Fig. 3.

antibody binding was observed in the tubulointerstitium of acatalasemic remnant kidneys at time points later than 6 weeks as compared to wild-type (Fig. 4D and E). Sham-treated kidneys gave only a trace of antibody reaction (Fig. 4A and B). 4-HHE staining peaked at 6 weeks after 5/6 nephrectomy and it remained high in the acatalasemic remnant kidneys through 18 weeks (Fig. 4F). Serum

malondialdehyde (MDA) levels detected by the TBARS method slightly increased in acatalasemia 18 weeks after 5/6 nephrectomy, without a significant difference from those of wild-type mice (data not shown). The extent of DNA damage has been evaluated by examination of urinary 8-OHdG excretion. In acatalasemic mice at time points later than 6 weeks after 5/6 nephrectomy, the urinary excretion of 8-OHdG was markedly higher than that in wild-type mice (Fig. 4G).

No significant compensation of glutathione peroxidase or SOD for catalase in acatalasemic remnant kidneys

The maintenance of tissue homeostasis requires an appropriate balance between oxidants and antioxidants. Two major antioxidant enzymes, catalase and glutathione peroxidase, are physiologically involved in the detoxification of H_2O_2 and thus protect tissues from oxidant-mediated injury. Therefore we next examined whether other antioxidant enzymes could compensate for catalase in acatalasemic remnant kidneys. Renal catalase activity from the acatalasemic mice exhibited a 4.6-fold ($P < 0.01$) decrease compared with wild-type mice at the start of the experiment, and remained low during the experimental period (Fig. 5A). The renal catalase activity in wild-type mice continued to decrease until 18 weeks following 5/6 nephrectomy. Since high catalase levels are found in erythrocytes [8], we compared the catalase activity between saline-perfused and unperfused kidneys after the removal of residual blood. The catalase activity of the perfused kidney was $6.0 \pm 0.2\%$ lower than that of the unperfused kidney [22]. To examine the effect of acatalasemia on other renal antioxidant enzymes in remnant kidneys, we investigated the activity of glutathione peroxidase (Fig. 5B) and SOD (Fig. 5C) in wild-type or acatalasemic mice. The activity of glutathione peroxidase showed a temporary decrease at 6 to 12 weeks after 5/6 nephrectomy; however, there was not any compensatory up0regulation of glutathione peroxidase in acatalasemic remnant kidneys or significant difference in glutathione peroxidase activities between the two mice groups (Fig. 5B). The level of SOD activity decreased during the development of renal failure and there were no significant changes in the activity of this enzyme between the two groups (Fig. 5C). Since SOD catalyzes the conversion of superoxide anion radical to H_2O_2 and O_2, it is suggested that the level of production of ROS mediated by SOD may be similar in the remnant kidneys in the two groups of mice.

A membrane-permeable SOD mimetic, tempol, does not prevent peroxidation or tubulointerstitial fibrosis in catalase deficiency

Tempol has been reported to act as a SOD mimetic producing antioxidative activity in various biologic systems
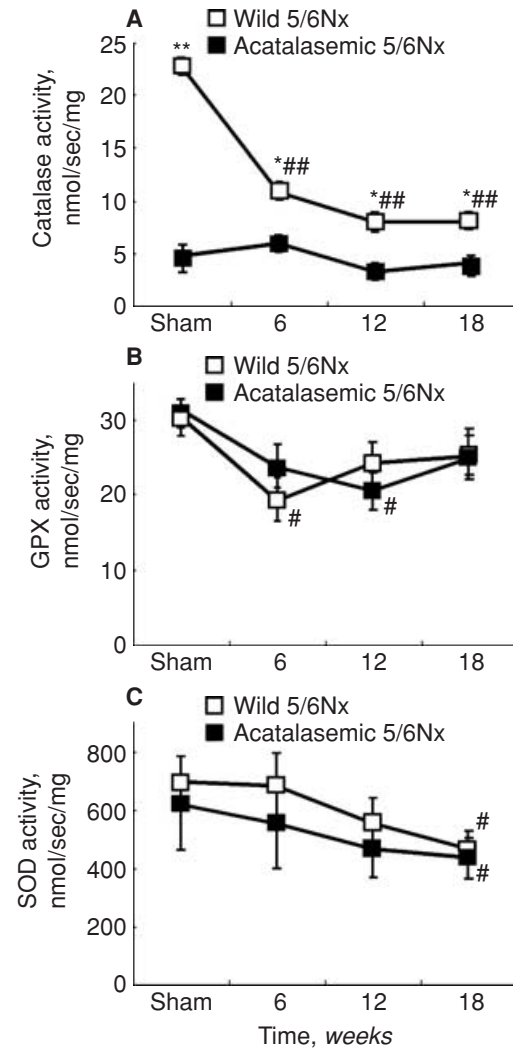
Fig. 5. Renal content of anti-oxidant enzymes in remnant kidneys of wild-type (□) and acatalasemic mice (■). Time courses of catalase (*A*), glutathione peroxidase (GPX) (*B*), and superoxide dismutase (SOD) (*C*) activities. Each enzyme activity is expressed as nmol/s/mg protein. Each column consists of means ± SE (*N* = 7 to 10 animals/group). *$P <$ 0.05; **$P <$ 0.01 vs. wild-type 5/6 nephrectomy (5/6Nx) mice at the same time point; #$P <$ 0.05; ##$P <$ 0.01 vs. sham at 0 week in the same group.

[39]. It is capable of dismuting superoxide anion radical to produce H_2O_2. We next investigated whether the SOD mimetic could prevent oxidant tissue injury in remnant kidneys (Table 4). Infusion of tempol significantly inhibited the daily urinary albumin excretion, renal deposition of HNE peroxidation products, and interstitial fibrosis in the wild-type mice at 12 weeks after 5/6 nephrectomy. However, the superoxide dismutation by tempol exacerbated albuminuria or oxidant-mediated renal fibrosis in the acatalasemic mice after 5/6 nephrectomy (Table 4), suggesting this SOD mimetic may not be utilized as an antioxidant under excessive oxidative stress in the acatalasemic kidney.

Table 4. Effect of tempol on remnant kidney model at 12 weeks

Group	Vehicle	Tempol
Urinary albumin to creatinine excretion ratio		
Wild-type 5/6 nephrectomy	0.72 ± 0.12	0.44 ± 0.08[a]
Acatalasemic 5/6 nephrectomy	2.29 ± 0.70[b]	3.77 ± 0.49[a,c]
HNE staining score		
Wild-type 5/6 nephrectomy	1.23 ± 0.21	1.00 ± 0.25[a]
Acatalasemic 5/6 nephrectomy	2.45 ± 0.32[b]	2.71 ± 0.18[a,b]
Interstitial fibrosis score		
Wild-type 5/6 nephrectomy	1.98 ± 0.30	1.47 ± 0.08[a]
Acatalasemic 5/6 nephrectomy	2.81 ± 0.19[b]	3.48 ± 0.14[a,b]

Values are means ± SE of 8 to 10 animals in each group.
[a]$P < 0.05$ vs. vehicle-treated group; [b]$P < 0.05$; [c]$P < 0.01$ vs. wild-type 5/6 nephrectomy in the same treatment group.

DISCUSSION

In the present study, acatalasemic mice strains deficient in catalase activity were used as the animal model. These mice were found to be more susceptible to functional and morphologic alterations in kidneys induced by 5/6 nephrectomy than wild-type mice. The level of albuminuria in the acatalasemic mice after 5/6 nephrectomy was significantly higher than that in wild-type mice. Urinary and renal peroxidation products increased in the acatalasemic mice after 5/6 nephrectomy as compared to wild-type mice. Interstitial fibrosis with an increased accumulation of type I and type IV collagens was more prominent in the acatalasemic than wild-type remnant kidneys. The acceleration of tubular EMT, a key event in renal fibrogenesis, was observed in acatalasemic mice after 5/6 nephrectomy in association with an elevation of EMT-regulated genes. Renal catalase activity remained low without compensatory up-regulation of glutathione peroxidase or SOD. Moreover, supplementation of tempol, a membrane-permeable SOD mimetic, did not prevent oxidant-mediated renal fibrosis in catalase deficiency. Collectively, the data suggest that ROS, particularly hydroxyl radical in the reduction of catalase activity, may be involved in the acceleration of EMT and renal fibrogenesis found in acatalasemic disease conditions.

Tissue fibrosis is considered to be a final outcome characteristic of chronic organ injury. The process of organ fibrosis includes the production of cytokines and chemokines, migration of inflammatory cells into the inflamed sites, activation of fibroblasts to produce ECM, regeneration of damaged tissue via cell proliferation and differentiation, and finally ECM remodeling [40]. Mature TECs in the adult kidney undergo EMT, a phenotype conversion that is fundamentally linked to the pathogenesis of renal tubulointerstitial fibrosis. In the current study, we have sought evidence of phenotypic alteration of TECs in the remnant kidney model of acatalasemic mice (Fig. 3). De novo expression of actin fibers in the cytoplasm of TECs adjacent to interstitial fibrosis (Fig. 3A and B) and a remarkable up-regulation of α-SMA genes (Fig. 3C)

were observed in remnant kidneys of the acatalasemic mice after 5/6 nephrectomy. In terms of the regulation of EMT, TGF-β1 [18] and CTGF [19] are considered to play profibrotic roles. BMP-7 [17, 20] and HGF [21] are candidate antifibrotic molecules which might reverse EMT. Crucial roles for integrin-linked kinase, an intracellular serine/threonine protein kinase that interacts with the cytoplasmic domains of the β integrins in the regulation of cell shape change [41] and with Smad signaling proteins [42] in mediating tubular EMT, have also been reported. Interestingly, H_2O_2 inhibited the expression of c-met, a receptor for HGF in mouse renal TECs [43]. Therefore, the data reported here support a role for H_2O_2 and hydroxyl radical in the promotion of tubular EMT and renal fibrosis by suppressing the HGF-c-met interaction. Moreover, a recent in vitro study suggests that H_2O_2 induces α-SMA expression, fibronectin secretion, and decreased E-cadherin expression in rat proximal TECs and that it may thus play an important role in TGF-β1–induced EMT [44]. We demonstrated the up-regulation of the TGF-β1 and FSP-1 genes in remnant kidneys of acatalasemic mice after 5/6 nephrectomy (Fig. 3). Since the up-regulation of TGF-β1 and FSP-1 is merely a reflection of the myofibroblast-like phenotype, the possibility remains that it is the activated fibroblast, rather than TECs undergoing EMT, which serves as a source of TGF-β1 and FSP-1. A recent report suggests that about 36% of new fibroblasts come from local EMT, about 14% to 15% from the bone marrow, and the rest from local proliferation in renal fibrogenesis [32].

There is a discrepancy between the early development of the tubulointerstitial fibrosis in the kidney at 6 weeks (Fig. 2) and the relatively late progression of glomerulosclerosis at 12 weeks (Table 3) in acatalasemic mice. The distribution of catalase is largely in the proximal tubules in the kidney, and less in the distal tubules, Henle's loops, and the collecting duct tubules or the glomeruli. The expression of catalase in mice is stronger in the proximal tubules in the juxtamedullary cortex rather than in the superficial cortex as detected by immunohistochemistry [45]. This may partly explain the findings that tubulointerstitial fibrosis is observed in a periglomerular pattern and is prominent in the deep cortex in the acatalasemic mice after 5/6 nephrectomy. It is speculated that glomerulosclerosis may develop in the late stage as a consequence of the tubulointerstitial injury in acatalasemia.

A significant albuminuria was observed and was associated with decline in renal function and with tubulointerstitial fibrosis in acatalasemic mice after 5/6 nephrectomy. The capacity of oxidants to impair the glomerular filtration barrier and give rise to increased rates of urinary albumin excretion has been reported [46]. When H_2O_2 was infused into the renal artery to achieve renal concentrations in the low micromolar range, it gave rise to an explosive, 50-fold increase in urinary albumin excretion

without a hemodynamic effect or ultrastructural abnormalities of the glomerular basement membrane [46]. The renal proximal TECs activated by reabsorption of filtrated albumin are thought to play an important role in the generation of ROS in kidney disease. Albumin per se can generate intracellular ROS in proximal TECs, which are responsible for the activation of certain redox-sensitive transcription factors, including nuclear factor-κB (NF-κB) [47] and signal transducers and activators of transcription (STAT5) [48]. Since the localization of catalase in the kidney is mainly in the proximal tubules [45], an overexposure of albumin to proximal TECs may induce an oxidant burst in the acatalasemic tubular cells, which subsequently conduct differential gene expression and phenotypic alteration, including cell differentiation. The interaction of albumin with the endocytosis receptors megalin and cubilin of the proximal TECs may lead to the generation of intracellular ROS [49]. We investigated the expression of megalin in acatalasemic tubules after 5/6 nephrectomy by immunohistochemistry; however, the expression level was comparable to that seen in the wild-type mice (data not shown). Absorbed albumin is degraded by lysosomal enzymes such as cathepsin B and L in TECs. The inability to degrade albumin in lysosomal disorders can result in the accumulation of albumin in TECs and subsequent cell injury [50]. Taken together, although we cannot rule out the possibility that tubulointerstitial fibrosis in acatalasemic mice is a secondary event, the albuminuria which developed in acatalasemic mice after 5/6 nephrectomy could well induce excess ROS in TECs, which would then lead to tubular injury.

Catalase and glutathione peroxidase are two major antioxidant enzymes involved in the degradation of H_2O_2 into nontoxic water and oxygen. Glutathione peroxidase constitutes as a high affinity and low capacity degradative system, whereas catalase represents in contrast a relatively low affinity and high capacity system. Glutathione peroxidase constitutes the first, and catalase the second line of defense against the buildup of H_2O_2. The two enzymes act in a complementary fashion to metabolize H_2O_2 generated in the course of both normal metabolic and disease processes in the kidney. We first speculated that glutathione peroxidase or SOD might compensate for the catalase deficiency in acatalasemic remnant kidneys; however, no compensatory up-regulation of glutathione peroxidase or SOD were evident in remnant kidney. The supplementation of a membrane-permeable SOD mimetic tempol, utilized as an antioxidant, did not prevent peroxidation or tubulointerstitial fibrosis in the acatalasemic remnant kidneys (Table 4). Recent reports have indicated that this SOD mimetic increases the formation of H_2O_2 and the increased H_2O_2, thereby, counteracts its biologic actions in renal medulla [51, 52]. Our data suggest that tempol may not be utilized as an antioxidant under excessive oxidative stress in the acatalasemia.

Tempol would be expected to be able to effectively reduce oxidative stress if the catalase activity is sufficient in the tissue.

Hypertension has important influence on the progression of renal diseases and glomerulosclerosis. In the present study, the blood pressure in the acatalasemic mice increased slightly after 5/6 nephrectomy without significant difference compared to baseline blood pressure (Table 2). The renal ablation model has been well-characterized in different rat strains. In contrast, mice have generally been resistant to this model. The paper by Kren and Hostetter [38] demonstrated that no significant differences were noted in blood pressure, proteinuria, or histopathology including glomerulosclerosis between control mice and mice after 5/6 nephrectomy induced by renal artery ligation in a C57BL/6 background. Subsequently, Ma and Fogo [53] reported that in 129/Sv mice with two renin genes and higher plasma renin activity, blood pressure increased significantly after 5/6 nephrectomy. They also speculated that the superior effects of renal artery ligation plus cautery may result from higher blood pressure responses. The pole resection protocol utilized in this study may result in lower blood pressure than the ligation plus cautery protocol. Moreover, the C3H/AnL background may not be susceptible to systemic hypertension even if the mice are systemically acatalasemic. Direct infusion of H_2O_2 into the renal medulla resulted in an increase in blood pressure [51]. A threefold elevation of the renal medullary interstitial H_2O_2 level (to approximately 600 nmol/L) was necessary to induce hypertension. In the current study, the concentration of H_2O_2 in the renal tubulointerstitium might not have been sufficient to increase the blood pressure in acatalasemic mice after 5/6 nephrectomy, although we did not check the concentration of H_2O_2.

At present there are few reports on the long-term health effects of functional catalase deficiency in humans. A high incidence of diabetes mellitus and deleterious changes in lipid and carbohydrate metabolism have recently been reported in Hungarian patients with acatalasemia, suggesting that this inherited disorder may be one of the risk factors for the development of diabetes mellitus and atherosclerosis [54]. Catalase deficiency may also predispose to cumulative oxidant damage in human pancreatic beta cells. Indeed, a preliminary study suggested that acatalasemic mice are more susceptible to the hyperglycemia induced by diabetogenic compound alloxan as compared to wild-type mice (unpublished observations). However, the effect of acatalasemia on the progression of kidney disease has been poorly understood, with no definitive reports of renal fibrosis in patients with acatalasemia in the literature. The findings presented here should provide an important first step toward obtaining the necessary mechanistic insights to enable treatment of such patients.

CONCLUSION

Acatalasemia sensitizes remnant kidneys to albuminuria and tubulointerstitial fibrosis by excessive oxidative stress and the promotion of tubular EMT. Suppression or detoxification of ROS is put forward as a possible means to reverse tubular EMT and the subsequent fibrosis of the kidney. Consequently, future work on the elucidation and development of novel therapeutic strategies, including the overexpression of catalase and specific quenching of hydroxyl radical to inhibit ROS-mediated EMT and subsequent renal fibrosis in acatalasemia, is urgently required. Moreover, an in vitro study to elucidate whether cultured renal TECs acquire a mesenchymal phenotype on exposure to H_2O_2 in association with TGF-β and CTGF expression is required and remains to be carried out.

REFERENCES

1. PINZANI M, ROMBOUTS K: Liver fibrosis: from the bench to clinical targets. *Dig Liver Dis* 36:231–242, 2004
2. COOPER ME: The role of the renin-angiotensin-aldosterone system in diabetes and its vascular complications. *Am J Hypertens* 17:S16–S20, 2004
3. HAUGEN E, NATH KA: The involvement of oxidative stress in the progression of renal injury. *Blood Purif* 17:58–65, 1999
4. SHIOMI T, TSUTSUI H, MATSUSAKA H, *et al*: Overexpression of glutathione peroxidase prevents left ventricular remodeling and failure after myocardial infarction in mice. *Circulation* 109:544–549, 2004
5. CHANCE B, SIES H, BOVERIS A: Hydroperoxide metabolism in mammalian organs. *Physiol Rev* 59:527–605, 1979
6. OSHINO N, OSHINO R, CHANCE B: The characteristics of the "peroxidatic" reaction of catalase in ethanol oxidation. *Biochem J* 131:555–563, 1973
7. TAKAHARA S: Acatalasemia. *Lancet* 2:1101–1106, 1952
8. OGATA M: Acatalasemia. *Hum Genet* 86:331–340, 1991
9. FEINSTEIN RN, SUTER H, JAROSLOW BN: Blood catalase polymorphism: Some immunological aspects. *Science* 159:638–640, 1968
10. SHAFFER JB, SUTTON RB, BEWLEY GC: Isolation of a cDNA clone for murine catalase and analysis of an acatalasemic mutant. *J Biol Chem* 262:12908–12911, 1987
11. HO YS, XIONG Y, MA W, *et al*: Mice lacking catalase develop normally but show differential sensitivity to oxidant tissue injury. *J Biol Chem* 279:32804–32812, 2004
12. EDDY AA: Molecular basis of renal fibrosis. *Pediatr Nephrol* 15:290–301, 2000
13. REMUZZI G, RUGGENENTI P, PERICO N: Chronic renal diseases: Renoprotective benefits of renin-angiotensin system inhibition. *Ann Intern Med* 136:604–615, 2002
14. EL-NAHAS AM: Plasticity of kidney cells: Role in kidney remodeling and scarring. *Kidney Int* 64:1553–1563, 2003
15. NG YY, HUANG TP, YANG WC, *et al*: Tubular epithelial-myofibroblast transdifferentiation in progressive tubulointerstitial fibrosis in 5/6 nephrectomized rats. *Kidney Int* 54:864–876, 1998
16. STRUTZ F, OKADA H, LO CW, *et al*: Identification and characterization of a fibroblast marker: FSP1. *J Cell Biol* 130:393–405, 1995
17. KALLURI R, NEILSON EG: Epithelial-mesenchymal transition and its implications for fibrosis. *J Clin Invest* 112:1776–1784, 2003
18. FAN JM, NG YY, HILL PA, *et al*: Transforming growth factor-beta regulates tubular epithelial-myofibroblast transdifferentiation in vitro. *Kidney Int* 56:1455–1467, 1999
19. INOUE T, OKADA H, KOBAYASHI T, *et al*: Hepatocyte growth factor counteracts transforming growth factor-beta1, through attenuation of connective tissue growth factor induction, and prevents renal fibrogenesis in 5/6 nephrectomized mice. *FASEB J* 17:268–270, 2003
20. ZEISBERG M, KALLURI R: The role of epithelial-to-mesenchymal transition in renal fibrosis. *J Mol Med* 82:175–181, 2004
21. LIU Y: Epithelial to mesenchymal transition in renal fibrogenesis: pathologic significance, molecular mechanism, and therapeutic intervention. *J Am Soc Nephrol* 15:1–12, 2004
22. SUNAMI R, SUGIYAMA H, WANG DH, *et al*: Acatalasemia sensitizes renal tubular epithelial cells to apoptosis and exacerbates renal fibrosis after unilateral ureteral obstruction. *Am J Physiol Renal Physiol* 286:F1030–F1038, 2004
23. SUGIYAMA H, KASHIHARA N, MAKINO H, *et al*: Apoptosis in glomerular sclerosis. *Kidney Int* 49:103–111, 1996
24. HASHIMOTO N, MAESHIMA Y, SATOH M, *et al*: Overexpression of angiotensin type 2 receptor ameliorates glomerular injury in a mouse remnant kidney model. *Am J Physiol Renal Physiol* 286:F516–F525, 2004
25. SUGAYA T, NISHIMATSU S, TANIMOTO K, *et al*: Angiotensin II type 1a receptor-deficient mice with hypotension and hyperreninemia. *J Biol Chem* 270:18719–18722, 1995
26. TOYOKUNI S, TANAKA T, HATTORI Y, *et al*: Quantitative immunohistochemical determination of 8-hydroxy-2′-deoxyguanosine by a monoclonal antibody N45.1: Its application to ferric nitrilotriacetate-induced renal carcinogenesis model. *Lab Invest* 76:365–374, 1997
27. SATOH M, KASHIHARA N, YAMASAKI Y, *et al*: Renal interstitial fibrosis is reduced in angiotensin II type 1a receptor-deficient mice. *J Am Soc Nephrol* 12:317–325, 2001
28. MAKINO H, SUGIYAMA H, YAMASAKI Y, *et al*: Glomerular cell apoptosis in human lupus nephritis. *Virchows Arch* 443:67–77, 2003
29. SUZUKI J, OTSUKA F, INAGAKI K, *et al*: Novel action of activin and bone morphogenetic protein in regulating aldosterone production by human adrenocortical cells. *Endocrinology* 145:639–649, 2004
30. XU J, SMOCK SL, SAFADI FF, *et al*: Cloning the full-length cDNA for rat connective tissue growth factor: Implications for skeletal development. *J Cell Biochem* 77:103–115, 2000
31. KAWADA N, MORIYAMA T, ANDO A, *et al*: Role of intron 1 in smooth muscle alpha-actin transcriptional regulation in activated mesangial cells in vivo. *Kidney Int* 55:2338–2348, 1999
32. IWANO M, PLIETH D, DANOFF TM, *et al*: Evidence that fibroblasts derive from epithelium during tissue fibrosis. *J Clin Invest* 110:341–350, 2002
33. MASUOKA N, WAKIMOTO M, OHTA J, *et al*: Characterization of hydrogen peroxide removal activities in mouse hemolysates: Catalase activity and hydrogen peroxide removal activity by hemoglobin. *Biochim Biophys Acta* 1361:131–137, 1997
34. MASUOKA N, KODAMA H, ABE T, *et al*: Characterization of hydrogen peroxide removal reaction by hemoglobin in the presence of reduced pyridine nucleotides. *Biochim Biophys Acta* 1637:46–54, 2003
35. WAKIMOTO M, MASUOKA N, NAKANO T, UBUKA T: Determination of glutathione peroxidase activity and its contribution to hydrogen peroxide removal in erythrocytes. *Acta Med Okayama* 52:233–237, 1998
36. SUTHERLAND MW, LEARMONTH BA: The tetrazolium dyes MTS and XTT provide new quantitative assays for superoxide and superoxide dismutase. *Free Radic Res* 27:283–289, 1997

37. KAIMORI JY, TAKENAKA M, NAKAJIMA H, *et al*: Induction of glia maturation factor-beta in proximal tubular cells leads to vulnerability to oxidative injury through the p38 pathway and changes in antioxidant enzyme activities. *J Biol Chem* 278:33519–33527, 2003

38. KREN S, HOSTETTER TH: The course of the remnant kidney model in mice. *Kidney Int* 56:333–337, 1999

39. SCHNACKENBERG CG, WELCH WJ, WILCOX CS: Normalization of blood pressure and renal vascular resistance in SHR with a membrane-permeable superoxide dismutase mimetic: Role of nitric oxide. *Hypertension* 32:59–64, 1998

40. LIU Y: Hepatocyte growth factor in kidney fibrosis: Therapeutic potential and mechanisms of action. *Am J Physiol Renal Physiol* 287:F7–F16, 2004

41. LI Y, YANG J, DAI C, *et al*: Role for integrin-linked kinase in mediating tubular epithelial to mesenchymal transition and renal interstitial fibrogenesis. *J Clin Invest* 112:503–516, 2003

42. LI JH, ZHU HJ, HUANG XR, *et al*: Smad7 inhibits fibrotic effect of TGF-beta on renal tubular epithelial cells by blocking Smad2 activation. *J Am Soc Nephrol* 13:1464–1472, 2002

43. ZHANG X, LIU Y: Suppression of HGF receptor gene expression by oxidative stress is mediated through the interplay between Sp1 and Egr-1. *Am J Physiol Renal Physiol* 284:F1216–F1225, 2003

44. RHYU DY, YANG Y, HA H, *et al*: Role of reactive oxygen species in TGF-{beta}1–induced mitogen-activated protein kinase activation and epithelial-mesenchymal transition in renal tubular epithelial cells. *J Am Soc Nephrol* 16:667–675, 2005

45. ZHOU Z, KANG YJ: Cellular and subcellular localization of catalase in the heart of transgenic mice. *J Histochem Cytochem* 48:585–594, 2000

46. YOSHIOKA T, ICHIKAWA I, FOGO A: Reactive oxygen metabolites cause massive, reversible proteinuria and glomerular sieving defect without apparent ultrastructural abnormality. *J Am Soc Nephrol* 2:902–912, 1991

47. MORIGI M, MACCONI D, ZOJA C, *et al*: Protein overload-induced NF-kappaB activation in proximal tubular cells requires H_2O_2 through a PKC-dependent pathway. *J Am Soc Nephrol* 13:1179–1189, 2002

48. NAKAJIMA H, TAKENAKA M, KAIMORI JY, *et al*: Activation of the signal transducer and activator of transcription signaling pathway in renal proximal tubular cells by albumin. *J Am Soc Nephrol* 15:276–285, 2004

49. CHRISTENSEN EI, BIRN H: Megalin and cubilin: multifunctional endocytic receptors. *Nat Rev Mol Cell Biol* 3:256–266, 2002

50. OSICKA TM, KIRIAZIS Z, PRATT LM, *et al*: Ramipril and aminoguanidine restore renal lysosomal processing in streptozotocin diabetic rats. *Diabetologia* 44:230–236, 2001

51. MAKINO A, SKELTON MM, ZOU AP, COWLEY AW, JR.: Increased renal medullary H_2O_2 leads to hypertension. *Hypertension* 42:25–30, 2003

52. CHEN YF, COWLEY AW, JR., ZOU AP: Increased H_2O_2 counteracts the vasodilator and natriuretic effects of superoxide dismutation by tempol in renal medulla. *Am J Physiol Regul Integr Comp Physiol* 285:R827–R833, 2003

53. MA LJ, FOGO AB: Model of robust induction of glomerulosclerosis in mice: Importance of genetic background. *Kidney Int* 64:350–355, 2003

54. GOTH L, EATON JW: Hereditary catalase deficiencies and increased risk of diabetes. *Lancet* 356:1820–1821, 2000